Autofocusing in Computer Microscopy: Selecting the Optimal Focus Algorithm

YU SUN,[1]* STEFAN DUTHALER,[2] AND BRADLEY J. NELSON[2]
[1]*Advanced Micro and Nanosystems Laboratory, University of Toronto, Canada*
[2]*Institute of Robotics and Intelligent Systems, Swiss Federal Institute of Technology, (ETH-Zurich), Switzerland*

KEY WORDS autofocusing; microscopy; computer vision; focus algorithms; ranking

ABSTRACT Autofocusing is a fundamental technology for automated biological and biomedical analyses and is indispensable for routine use of microscopes on a large scale. This article presents a comprehensive comparison study of 18 focus algorithms in which a total of 139,000 microscope images were analyzed. Six samples were used with three observation methods (brightfield, phase contrast, and differential interference contrast (DIC)) under two magnifications (100× and 400×). A ranking methodology is proposed, based on which the 18 focus algorithms are ranked. Image preprocessing was also conducted to extensively reveal the performance and robustness of the focus algorithms. The presented guidelines allow for the selection of the optimal focus algorithm for different microscopy applications. *Microsc. Res. Tech. 65:139–149, 2004.*

INTRODUCTION

Autofocusing is a fundamental technology for automated biological and biomedical applications, such as in high-throughput screening for the pharmaceutical industry and in autonomous microrobotic cell manipulation. Reliable autofocusing methods are also indispensable for routine use of microscopes on a large scale, as in the microassembly of hybrid microelectromechanical systems (MEMS).

Although autofocusing is a long-standing topic in the literature and a variety of focus algorithms have been proposed, the selection of an appropriate focus algorithm for specific experimental microscopy conditions remains ad hoc and time-consuming. Based on the comparison results of 13 focus algorithms operating on fluorescence images, it was found by Santos et al. (1997) that AutoCorrelation (Vollath, 1987, 1988) is the optimal focus algorithm for fluorescence microscopy applications. However, AutoCorrelation was not found to be the optimal focus algorithm for microscopy images under brightfield, phase contrast, or differential interference contrast (DIC), thus motivating this study.

This article presents a systematic evaluation of 18 widely used focus algorithms and comprehensive comparison results by processing a total of 139,000 microscope images. Six samples were used in experiments with three observation methods (brightfield, phase contrast, and DIC) and two magnifications (100× and 400×). Besides the criteria of monotonicity and single modality for evaluating focus algorithms, three other criteria are adopted to systematically evaluate the performance of the 18 focus algorithms. In order to extensively study the performance of the focus algorithms, filtering (preprocessing) operations including subsampling, low-pass filtering, and random noise addition were conducted on images before the focus algorithms were applied. Based on the large amount of experimental data, the performance of the focus algorithms is analyzed and compared using individual criteria and an overall ranking is determined. Subsequently, guidelines for selecting the optimal focus algorithm are obtained.

MATERIALS AND METHODS

The six samples shown in Figure 1 were used in the experiments for testing the 18 focus algorithms and include adenomatosis of the colon, muscles of a baby snake, liver cells, pancreas cells, kidney cells, and ground stone. The thickness of the samples was 2–6 μm. These samples were chosen because they embody a variety of information, from which more general conclusions for selecting the optimal focus algorithm can be reached. The larger the information content, the easier the focusing.

The experimental setup consists of a motorized inverted microscope (Olympus IX81), a framegrabber (Matrox Meteor-II), and a CCD camera (Sony XC-HR50). The motorized inverted microscope has a minimum focus step of 0.01 μm. Two objectives were used, a 10× objective (Olympus UPlanFl, 3 μm depth of field, NA 0.3) and a 40× objective (Olympus LCPlanFl, 1 μm depth of field, NA 0.6). The microscope provides three observation methods, including brightfield, phase contrast, and DIC. Figure 2 shows pancreas cells (sample 4) under these three optical conditions.

The 100× image sets were obtained in 1-μm steps, amounting to 400 images per sample. The 400× image sets were obtained in 0.25-μm steps within a smaller range, amounting to 550 images per sample. Applying the three observation methods and two magnifications to the six samples, 36 image sets were obtained with

*Correspondence to: Yu Sun, Advanced Micro and Nanosystems Laboratory, University of Toronto, Toronto, M5S 3G8 Canada. E-mail: sun@mie.utoronto.ca
Yu Sun holds a cross-appointment at the Institute of Biomaterials and Biomedical Engineering.

Received 3 August 2004; accepted in revised form 10 October 2004
DOI 10.1002/jemt.20118
Published online in Wiley InterScience (www.interscience.wiley.com).

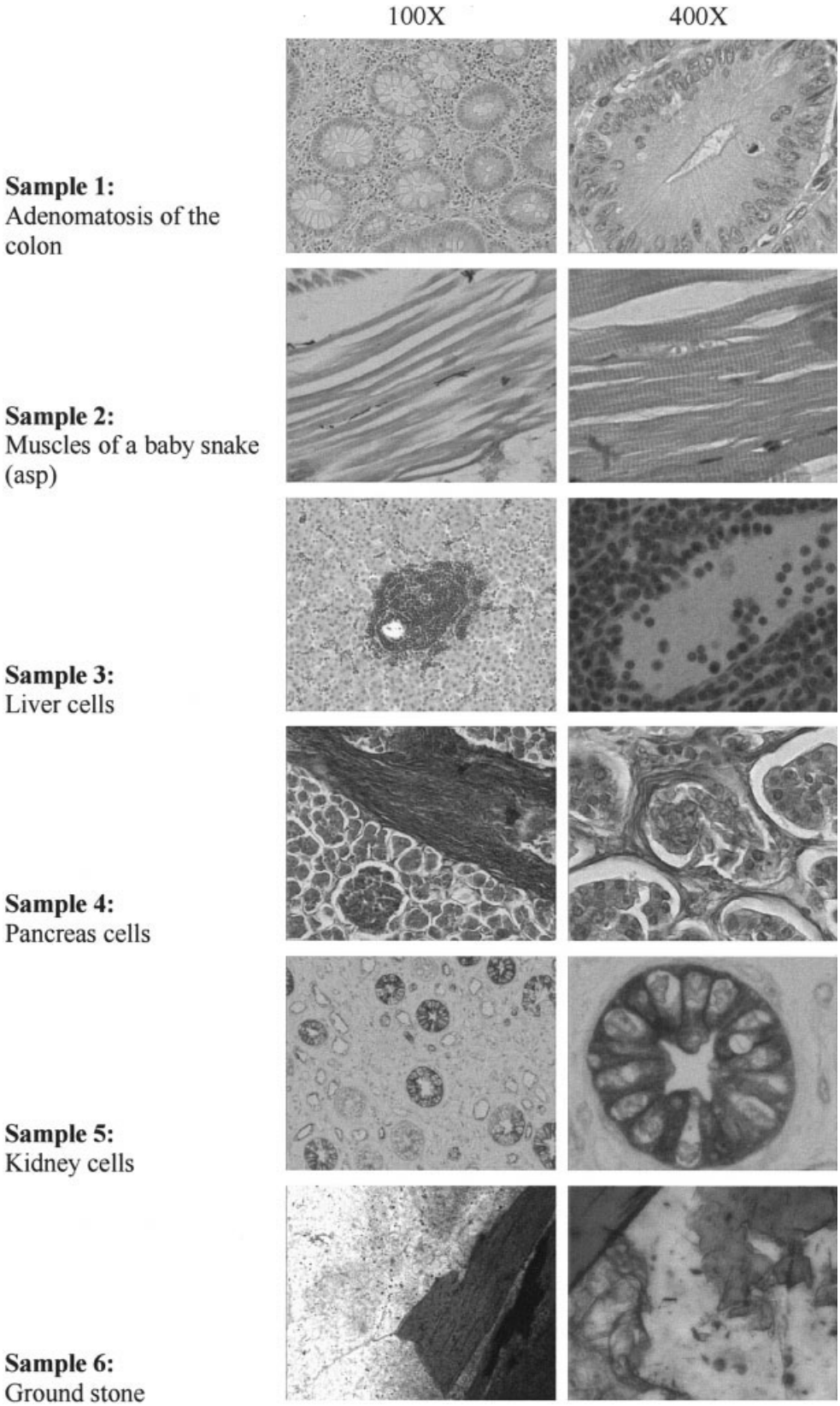

Fig. 1. Brightfield images of the recorded samples with 100× and 400× magnifications.

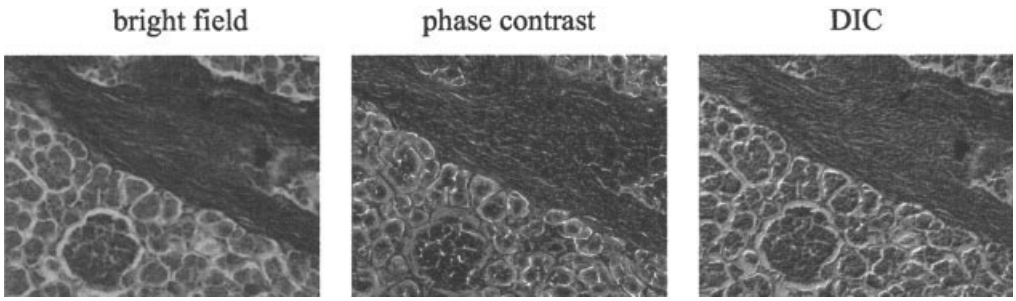

Fig. 2. Images of pancreas cells under brightfield, phase contrast, and differential interference contrast (DIC).

each set having either 400 images or 550 images. A total of 139,500 images were processed and analyzed.

The focus algorithms were implemented on a PC (2.53 GHz CPU and 512 MB RAM). Computation time, discussed in Results and Discussion, does not exceed 30 ms for almost all the focus algorithms tested. Therefore, the speed of the focus algorithms is not used as a criterion for comparing and ranking the 18 focus algorithms.

FOCUS ALGORITHMS

A variety of focus algorithms have been proposed and compared in the literature. The output of an ideal focus algorithm is defined as having a maximum value at the best-focused image/position and decreasing as defocus increases. Eighteen widely used focus algorithms in the literature were tested and compared in this study, which can be classified into four groups.

Derivative-Based Algorithms

These algorithms assume that well-focused images have more high-frequency content than defocused images. Neighboring pixels in images with high-frequency content have large differences in intensity. The larger these intensity changes, the sharper the edges. In order to apply high-pass filtering, these algorithms apply convolution masks to an image to obtain derivatives. Different norms are subsequently used to compute the magnitude of the derivative vectors. One disadvantage of these algorithms is that they are more sensitive to high-frequency noise.(获得高频信息)

Thresholded Absolute Gradient (Santos et al., 1997). This algorithm sums the absolute value of the first derivative that is larger than a threshold θ:

$$F_{th\_grad} = \sum_{Height} \sum_{Width} \left| i(x+1, y) - i(x, y) \right| \quad \text{(F-1)}$$

where $|i(x + 1, y) - i(x, y)| \geq \theta$, and $i(x, y)$ is the gray level intensity of pixel (x, y).

Squared Gradient (Santos et al., 1997). This algorithm sums squared differences, making larger gradients exert more influence.

$$F_{sq\_grad} = \sum_{Height} \sum_{Width} \left(i(x+1, y) - i(x, y) \right)^2 \quad \text{(F-2)}$$

where $\left(i(x + 1, y) - i(x, y) \right)^2 \geq \theta$.

Brenner Gradient (Brenner et al., 1971). This algorithm computes the first difference between a pixel and its neighbor with a horizontal/vertical distance of 2.

$$F_{Brenner} = \sum_{Height} \sum_{Width} \left(i(x+2, y) - i(x, y) \right)^2 \quad \text{(F-3)}$$

where $(i(x + 2, y) - i(x, y))^2 \geq \theta$.

Tenenbaum Gradient (Tenengrad) (Yeo et al., 1993; Krotov, 1987). This algorithm convolves an image with Sobel operators, and then sums the square of the gradient vector components.

$$F_{Tenengrad} = \sum_{Height} \sum_{Width} S_x(x, y)^2 + S_y(x, y)^2 \quad \text{(F-4)}$$

where $S_x(x, y)$ and $S_y(x, y)$ are the resultant images from convolution with the Sobel operators.

Sum of Modified Laplace (Nayar and Nakagawa, 1994). This algorithm sums the absolute values of the convolution of an image with Laplacian operators.

$$F_{SML} = \sum_{Height} \sum_{Width} \left| L_x(x, y) \right| + \left| L_y(x, y) \right| \quad \text{(F-5)}$$

Energy Laplace (Subbarao et al., 1993). This algorithm convolves an image with the convolution mask:

$$L = \begin{bmatrix} -1 & -4 & -1 \\ -4 & 20 & -4 \\ -1 & -4 & -1 \end{bmatrix}$$

to compute the second derivative $C(x, y)$. The final output is the sum of the squares of the convolution results.

$$F_{energy\_Laplace} = \sum_{Height} \sum_{Width} C(x, y)^2 \quad \text{(F-6)}$$

Wavelet Algorithm W_1 (Yang and Nelson, 2003a,b). This algorithm uses the Daubechies D6 wavelet filter, applying both high-pass (H) and low-pass (L) filtering to an image. The resultant image is divided into four subimages: LL, HL, LH, and HH. The algorithm sums the absolute values in the HL, LH, and HH regions.

$$F_{W1} = \sum_{Height}\sum_{Width}\left|W_{HL}(x,y)\right| + \left|W_{LH}(x,y)\right| + \left|W_{HH}(x,y)\right| \quad \text{(F-7)}$$

Wavelet Algorithm W_2 (Yang and Nelson, 2003a,b). This algorithm sums the variances in the HL, LH, and HH regions. The mean values μ in each region are computed from absolute values.

$$F_{W2} = \frac{1}{H\cdot W}\sum_{Height}\sum_{Width}\left(\left|W_{HL}(x,y)\right| - \mu_{LL}\right)^2 + \left(\left|W_{LH}(x,y)\right| - \mu_{LH}\right)^2 + \left(\left|W_{HH}(x,y)\right| - \mu_{HH}\right)^2 \quad \text{(F-8)}$$

where H and W are image height and width.

Wavelet Algorithm W_3 (Yang and Nelson, 2003a,b). This algorithm differs from [F-8] in that the mean values $\bar{\mu}$ in the HL, LH, and HH regions are computed without using absolute values.

$$F_{W3} = \frac{1}{H\cdot W}\sum_{Height}\sum_{Width}\left(W_{HL}(x,y) - \bar{\mu}_{LL}\right)^2 + \left(W_{LH}(x,y) - \bar{\mu}_{LH}\right)^2 + \left(W_{HH}(x,y) - \bar{\mu}_{HH}\right)^2 \quad \text{(F-9)}$$

Statistical Algorithms(图像本身存在的信息)

These statistics-based algorithms distinguish focused images from defocused images using variance and correlation. They are generally less sensitive to noise than derivative-based algorithms.

Variance (Groen et al., 1985; Yeo et al., 1993). This algorithm computes variations in gray level among image pixels. It uses the power function to amplify larger differences from the mean intensity μ instead of simply amplifying high-intensity values.

$$F_{variance} = \frac{1}{H\cdot W}\sum_{Height}\sum_{Width}\left(i(x,y) - \mu\right)^2 \quad \text{(F-10)}$$

Normalized Variance (Groen et al., 1985; Yeo et al., 1993). By normalizing the final output with the mean intensity μ, this algorithm compensates for the differences in average image intensity among different images.

$$F_{normed\_variance} = \frac{1}{H\cdot W\cdot \mu}\sum_{Height}\sum_{Width}\left(i(x,y) - \mu\right)^2 \quad \text{(F-11)}$$

AutoCorrelation (Vollath, 1987, 1988).

$$F_{auto\_corr} = \sum_{Height}\sum_{Width} i(x,y)\cdot i(x+1,y) - \sum_{Height}\sum_{Width} i(x,y)\cdot i(x+2,y) \quad \text{(F-12)}$$

Standard Deviation-Based Correlation (Vollath, 1987, 1988).

$$F_{corr\_stddev} = \sum_{Height}\sum_{Width} i(x,y)\cdot i(x+1,y) - H\cdot W\cdot \mu^2 \quad \text{(F-13)}$$

Histogram-Based Algorithms

These algorithms use histograms $h(i)$ (i.e., the number of pixels with intensity i in an image) to analyze the distribution and frequency of image intensities.

Range Algorithm (Firestone et al., 1991). This algorithm computes the difference between the highest and the lowest intensity levels.

$$F_{range} = \max_i(h(i)>0) - \min_i(h(i)>0) \quad \text{(F-14)}$$

Entropy Algorithm (Firestone et al., 1991). This algorithm assumes that focused images contain more information than defocused images.

$$F_{entropy} = -\sum_{intensities} p_i\cdot \log_2(p_i) \quad \text{(F-15)}$$

where $p_i = h(i)/H\cdot W$ is the probability of a pixel with intensity i.

Intuitive Algorithms

Thresholded Content (Groen et al., 1985; Mendelsohn and Mayall, 1972). This algorithm sums the pixel intensities above a threshold.

$$F_{th\_cont} = \sum_{Height}\sum_{Width} i(x,y) \quad \text{(F-16)}$$

where $i(x,y) \geq \theta$.

Thresholded Pixel Count (Groen et al., 1985). This algorithm counts the number of pixels having intensity below a given threshold.

$$F_{pixel\_count} = \sum_{Height}\sum_{Width} s\left(i(x,y),\theta\right) \quad \text{(F-17)}$$

where $s\left(i(x,y),\theta\right) = \begin{cases} 1, i(x,y)\leq\theta \\ 0, else \end{cases}$.

Image Power (Santos et al., 1997). This algorithm sums the square of image intensities above a given threshold.

$$F_{power} = \sum_{Height}\sum_{Width} i(x,y)^2 \quad \text{(F-18)}$$

where $i(x,y) \geq \theta$.

IMAGE PREPROCESSING

In order to test the behavior of the focus algorithms under different conditions, three approaches were individually used to preprocess images before a focus algorithm was applied.

Subsampling

Subsampling images increases execution speed because of reduced image data. Furthermore, it is also useful for testing a focus algorithm's robustness to image information reduction. In this study, a 50% subsampling means that every second pixel of an image is used both horizontally and vertically, resulting in one-fourth the input data.

Adding Random Noise

In order to investigate the influence of noise on the performance of the focus algorithms, a random noise filter was applied to the images.

Low-Pass Filtering

A binomial filter was used to preprocess images to reduce image noise levels and to investigate the overall impact of low-pass filtering on the performance of the focus algorithms. The convolution vector was constructed from the binomial numbers of Pascal's Triangle. For example, the convolution vector of size five is [1, 4, 6, 4, 1].

RANKING METHODOLOGY

Each focus algorithm produces a focus curve for an image set. In order to make valid comparisons, these focus curves were normalized and the curves inverted with their peak as the global minimum. The focus algorithms were evaluated using the following five criteria. The algorithms were ranked according to individual criteria as well as overall score.

Accuracy

This criterion measures the distance between the best focus position, manually determined by proficient microscope technicians, and the maximum of the focus curve. The smaller this measure is, the more accurate the focus algorithm.

Range

The range criterion describes the distance between two neighboring local minima around the global maximum. The larger this measure is, the easier it is to reach the global maximum without being trapped in a local maximum.

Number of False Maxima

This criterion describes the number of maxima appearing in a focus curve, excluding the global maximum.

Width

This criterion describes the sharpness/narrowness of the peak. The width of a curve at 50% of its height is computed as the width of the focus curve.

Noise Level

Criteria similar to the above four criteria have been adopted by Santos et al. (1997) for evaluating focus algorithm performance for fluorescence microscopy applications. Besides these four criteria, the noise level of a curve was also found to be important for autofocusing in this study. This criterion extends the false maximum criterion by describing the speed of the direction changes (second derivative) between two false maxima of a focus curve. As shown in Figure 3, the dashed curve is better than the solid curve because of the lower magnitude of the local peaks, although the two curves have the same number of false maxima. The lower deviation of the dashed curve from the ideal behavior increases the accuracy of approximation methods, such as forward Euler integration for adaptively setting step sizes and setting the next position of the microscope's Z-motor.

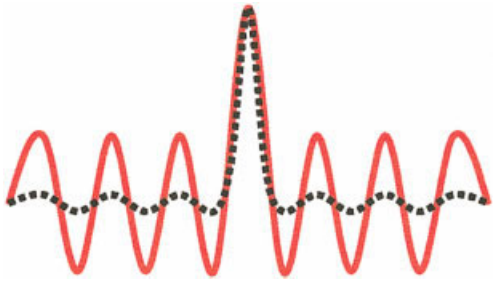

Fig. 3. Two artificial focus curves having the same number of false maxima but different noise level. The dashed curve is better in terms of scores in noise level. [Color figure can be viewed in the online issue, which is available at www.interscience.wiley.com.]

TABLE 1. Ideal values for each criterion in the ranking method

Criterion	accuracy	range	# of false max	width	noise level
Ideal Value	0	400/550	0	0	0

In order to quantitatively represent this criterion, the squares of the second derivatives are summed. The derivatives are obtained by convolving the focus curve with the Laplacian operator [–1, 2, –1]. The value at the peak is left out in order not to penalize algorithms with a small width.

Overall Score

For each focus curve produced by a focus algorithm, the difference/distance of each individual criterion (i.e., accuracy, range, number of false maximum, width, and noise level) from the corresponding ideal values is computed. The ideal values for each criterion are shown in Table 1. The ideal value for the range criterion is the total number of images in an image set. In this study, there are 400 images in an image set under 100× and 550 images in an image set under 400×.

Distances for each criterion from their ideal values are defined for a focus algorithm m as:

$$\begin{aligned} Dist_{accuracy}(m) &= accuracy(m) \\ Dist_{range}(m) &= maxRange - range(m) \\ Dist_{false\_maxima}(m) &= \#\ false\ maxima(m) \\ Dist_{width}(m) &= width(m) \\ Dist_{noise\_level}(m) &= noise\ level(m) \end{aligned} \quad (1)$$

TABLE 2. Ranking of the 18 focus algorithms according to individual criterion distances and overall score

Algorithm	Accuracy	Range	False max	Width	Noise level	Overall score
F-1 ThresholdAbsGrad	2.83 (6)	404.31 (8)	110.56 (12)	18.36 (5)	0.0229 (4)	1.1002 (7)
F-2 SquaredGradient	3.03 (8)	424.50 (11)	110.33 (11)	16.75 (4)	0.0360 (8)	1.1310 (8)
F-3 BrennerGradient	2.69 (2)	400.75 (6)	98.17 (8)	15.25 (3)	0.0305 (6)	1.0439 (5)
F-4 TenenbaumGradient	2.69 (2)	399.03 (4)	95.61 (7)	15.06 (2)	0.0284 (5)	1.0312 (4)
F-5 ModifiedLaplace	15.67 (12)	454.58 (13)	139.50 (16)	30.11 (6)	0.1412 (14)	1.3165 (14)
F-6 EnergyLaplace	14.64 (11)	450.19 (12)	127.75 (13)	30.53 (8)	0.0921 (12)	1.2585 (11)
F-7 Wavelet_1	16.03 (13)	457.17 (15)	142.06 (17)	30.33 (7)	0.1795 (16)	1.3324 (16)
F-8 Wavelet_2	29.47 (15)	458.47 (16)	129.03 (15)	49.92 (10)	0.1755 (15)	1.3190 (15)
F-9 Wavelet_3	22.83 (14)	456.50 (14)	128.92 (14)	41.64 (9)	0.1182 (13)	1.2936 (12)
F-10 Variance	2.78 (5)	153.64 (3)	14.33 (3)	51.92 (12)	0.0051 (3)	0.4131 (3)
F-11 NormedVariance	2.72 (4)	138.92 (1)	12.89 (2)	51.81 (11)	0.0050 (2)	0.3877 (1)
F-12 AutoCorrelation	2.67 (1)	410.19 (10)	106.47 (9)	14.08 (1)	0.0313 (7)	1.0915 (6)
F-13 StdDevCorr	2.83 (6)	148.75 (2)	12.58 (1)	53.28 (13)	0.0044 (1)	0.4070 (2)
F-14 Range	6.44 (10)	472.17 (17)	109.72 (10)	105.72 (17)	0.5969 (17)	1.3152 (13)
F-15 Entropy	5.22 (9)	482.97 (18)	156.17 (18)	72.25 (14)	3.6897 (18)	1.7662 (18)
F-16 AboveThreshold	56.22 (17)	403.75 (7)	51.78 (6)	105.22 (16)	0.0583 (10)	1.1889 (10)
F-17 PixelCount	94.06 (18)	408.31 (9)	45.78 (4)	211.67 (18)	0.0795 (11)	1.6736 (17)
F-18 ImagePower	55.22 (16)	400.39 (5)	51.25 (5)	94.64 (15)	0.0534 (9)	1.1575 (9)

Each entry is based on 36 image sets and averaged. For all the criterion distances in each column, a smaller value means better performance. The numbers in parenthesis represent the ranks of the focus algorithms. No image preprocessing was conducted.

TABLE 3. Ranking of the 18 focus algorithms according to individual criterion distances under 100× magnification

Algorithm	Accuracy	Range	False max	Width	Noise level	Overall score
F-1 ThresholdAbsGrad	0.44 (4)	339.83 (5)	88.28 (10)	10.44 (10)	0.0214 (4)	1.0444 (8)
F-2 SquaredGradient	0.44 (4)	363.22 (10)	91.89 (12)	6.83 (5)	0.0444 (11)	1.1036 (10)
F-3 BrennerGradient	0.39 (2)	349.33 (7)	77.61 (8)	7.50 (6)	0.0366 (10)	1.0137 (6)
F-4 TenenbaumGradient	0.39 (2)	350.00 (8)	75.17 (7)	7.72 (9)	0.0330 (8)	1.0048 (5)
F-5 ModifiedLaplace	0.56 (9)	382.89 (13)	114.33 (16)	6.67 (4)	0.0555 (12)	1.2483 (14)
F-6 EnergyLaplace	0.61 (13)	382.78 (12)	110.00 (13)	5.39 (1)	0.0767 (14)	1.2262 (11)
F-7 Wavelet_1	0.56 (9)	385.44 (14)	117.44 (17)	6.50 (3)	0.0620 (13)	1.2687 (15)
F-8 Wavelet_2	0.50 (7)	387.39 (15)	112.28 (15)	7.50 (6)	0.1022 (16)	1.2462 (12)
F-9 Wavelet_3	0.56 (9)	388.06 (16)	112.17 (14)	5.83 (2)	0.0894 (15)	1.2464 (13)
F-10 Variance	0.50 (7)	155.11 (3)	11.61 (3)	45.50 (12)	0.0072 (3)	0.4636 (3)
F-11 NormedVariance	0.44 (4)	131.94 (1)	8.83 (1)	45.44 (11)	0.0071 (2)	0.4171 (1)
F-12 AutoCorrelation	0.33 (1)	358.39 (9)	81.50 (9)	7.67 (8)	0.0344 (9)	1.0480 (9)
F-13 StdDevCorr	0.56 (9)	150.94 (2)	10.39 (2)	47.56 (13)	0.0061 (1)	0.4614 (2)
F-14 Range	3.00 (14)	408.67 (17)	90.94 (11)	107.56 (17)	0.5626 (17)	1.3514 (16)
F-15 Entropy	3.06 (15)	420.33 (18)	134.11 (18)	54.50 (14)	3.8237 (18)	1.7617 (18)
F-16 AboveThreshold	21.44 (17)	339.94 (6)	46.72 (5)	81.83 (16)	0.0226 (5)	1.0335 (7)
F-17 PixelCount	86.00 (18)	368.94 (11)	38.28 (4)	170.44 (18)	0.0306 (7)	1.6888 (17)
F-18 ImagePower	20.56 (16)	332.28 (4)	46.89 (6)	67.83 (15)	0.0293 (6)	0.9812 (4)

Each entry is based on 18 image sets and averaged. No image preprocessing was conducted.

TABLE 4. Ranking of the 18 focus algorithms according to individual criterion distances under 400× magnification

Algorithm	Accuracy	Range	False max	Width	Noise level	Overall score
F-1 ThresholdAbsGrad	5.22 (7)	468.78 (10)	132.83 (12)	26.28 (4)	0.0244 (5)	1.1433 (7)
F-2 SquaredGradient	5.61 (8)	485.78 (11)	128.78 (10)	26.67 (5)	0.0276 (7)	1.1528 (8)
F-3 BrennerGradient	5.00 (1)	452.17 (6)	118.72 (8)	23.00 (3)	0.0244 (6)	1.0683 (5)
F-4 TenenbaumGradient	5.00 (1)	448.06 (5)	116.06 (7)	22.39 (2)	0.0237 (4)	1.0529 (4)
F-5 ModifiedLaplace	30.78 (12)	526.28 (14)	164.67 (16)	53.56 (6)	0.2269 (14)	1.3870 (14)
F-6 EnergyLaplace	28.67 (11)	517.61 (12)	145.50 (13)	55.67 (8)	0.1076 (11)	1.3018 (10)
F-7 Wavelet_1	31.50 (13)	528.89 (15)	166.67 (17)	54.17 (7)	0.2970 (16)	1.4008 (15)
F-8 Wavelet_2	58.44 (15)	529.56 (16)	145.78 (15)	92.33 (14)	0.2489 (15)	1.4411 (16)
F-9 Wavelet_3	45.11 (14)	524.94 (13)	145.67 (14)	77.44 (12)	0.1469 (13)	1.3727 (12)
F-10 Variance	5.06 (5)	152.17 (3)	17.06 (3)	58.33 (10)	0.0030 (3)	0.3776 (3)
F-11 NormedVariance	5.00 (1)	145.89 (1)	16.94 (2)	58.17 (9)	0.0030 (2)	0.3686 (1)
F-12 AutoCorrelation	5.00 (1)	462.00 (7)	131.44 (11)	20.50 (1)	0.0283 (8)	1.1269 (6)
F-13 StdDevCorr	5.11 (6)	146.56 (2)	14.78 (1)	59.00 (11)	0.0028 (1)	0.3687 (2)
F-14 Range	9.89 (10)	535.67 (17)	128.50 (9)	103.89 (15)	0.6312 (17)	1.3013 (9)
F-15 Entropy	7.39 (9)	545.61 (18)	178.22 (18)	90.00 (13)	3.5557 (18)	1.7697 (18)
F-16 AboveThreshold	91.00 (17)	467.56 (8)	56.83 (6)	128.61 (17)	0.0940 (10)	1.3746 (13)
F-17 PixelCount	102.11 (18)	447.67 (4)	53.28 (4)	252.89 (18)	0.1285 (12)	1.6625 (17)
F-18 ImagePower	89.89 (16)	468.50 (9)	55.61 (5)	121.44 (16)	0.0775 (9)	1.3567 (11)

Each entry is based on 18 image sets and averaged. No image preprocessing was conducted.

Consequently, an optimum focus curve is at [0, 0, 0, 0, 0] in terms of criterion distances. In order to give all the distances equal weights, the criterion distances are all normalized. The lower a criterion distance, the better the performance of a focus algorithm under this criterion. The overall score is defined as the Euclidean

distance of a focus curve to [0, 0, 0, 0, 0]. The lower this overall score, the better the overall performance of a focus algorithm.

$$score(m) = \sqrt{\sum_{criteria} Dist_{criterion}(m)^2} \quad (2)$$

RESULTS AND DISCUSSION

A total of 139,000 images were obtained on the six samples that were observed under three observation conditions (i.e., brightfield, phase contrast, and DIC) and two magnifications (100× and 400×). A threshold of 150 was set for focus algorithms (F-15–F-18) because these algorithms exhibit satisfactory behavior with this threshold value. No threshold was set for the gradient-based focus algorithms (F-1–F-4) because threshold variation was not found to produce significant performance differences for these focus algorithms.

With criterion distances and the overall score defined in Eqs. (1, 2), *lower* values in all columns of the tables in this section represent *better* performance. The numbers in parentheses represent ranking of a focus algorithm according to individual criterion distances or the overall score.

Without Image Preprocessing

Lumping Observation Methods and Magnifications. Table 2 shows the performance and ranks of the 18 focus algorithms without image preprocessing according to individual criterion distances and the overall score. Each entry in the table is based on 36 image sets and averaged. One can see that Normalized Variance (F-11) and Standard-Deviation-Based Correlation (F-13) have the best range, least number of false maxima, and the lowest noise level. By lumping the three observation methods and two magnifications and without applying image preprocessing, Normalized Variance (F-11) was found to provide the best overall performance.

Under Different Magnifications. Data shown in Tables 3 and 4 were collected to investigate performance changes of the focus algorithms under different magnifications. No image preprocessing was conducted. The three observation methods were lumped together. Each entry in the tables is based on 18 image sets and averaged. By comparing the corresponding entries in Tables 3 and 4, one can see that accuracy, range, number of false maxima, width, and noise level are almost consistently improved for all the focus algorithms under 100× magnification than under 400× magnification. In terms of the overall score, magnification differences do not significantly change the ranking of the focus algorithms. For example, Normalized Variance (F-11) provides the best overall performance under both 100× and 400× magnifications.

As shown in Table 3 (also see Table 8), wavelet-based focus algorithms have small widths, but they always have local maxima around the global peak, which can be seen from the poor range distance. The small widths of the wavelet-based algorithms are due to the localized support property of wavelet basis, which makes them well suitable for image segmentation purposes (Yang and Nelson, 2003a).

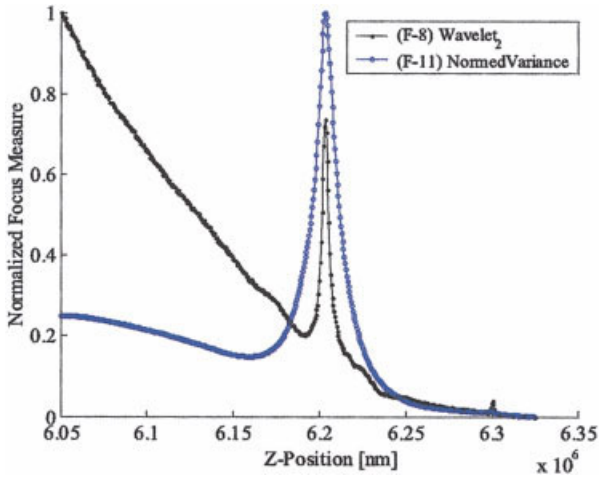

Fig. 4: Wavelet-based algorithm (F-8) with a misleading global maximum at the starting point. This undesired behavior only appears under 400× magnification, which also disappears as subsampling is applied to images (see Table 8). [Color figure can be viewed in the online issue, which is available at www.interscience.wiley.com.]

By comparing Tables 3 and 4, one can see that the accuracy of Laplace (F-5 and F-6) and Wavelet-based algorithms (F-7, F-8, and F-9) significantly deteriorates under 400×. This occurs because these algorithms have a misleading global maximum at the starting point, as shown in Figure 4. It should be noted that this undesired behavior only appears under 400× magnification, which also disappears as subsampling is applied to images (see Table 8).

Using Different Observation Methods. In order to investigate performance differences caused by observation methods, each criterion distance was computed based on 18 image sets for brightfield, phase contrast, and DIC images. One can see from Tables 5, 6, and 7 that most focus algorithms produce better accuracy under phase contrast than under brightfield and DIC. It was also found in experiments that DIC images appear very similar to the gradient images under brightfield, which improves the performance of the Image Power algorithm (F-18). This can be seen by comparing the last rows of Tables 5, 6, and 7. The improvement is due to the fact that Image Power (F-18) behaves similarly on DIC images as the squared gradient algorithm (F-2) on brightfield images. By comparing the overall scores, Normalized Variance (F-11) was found to provide the best overall performance under all the three observation methods.

Interestingly, it was found that all the focus curves under phase contrast have two local peaks around the global peak (Fig. 5) due to the phase transition effect. The two local peaks limit the range of all the focus algorithms, without which the focus algorithms would be capable of producing much larger ranges (i.e., lower range distances).

With Image Preprocessing

In order to investigate the influence of image preprocessing on the performance of the focus algorithms, the following preprocessing operations were individually applied:

TABLE 5. Ranking of the 18 focus algorithms according to individual criterion distance and overall score

Algorithm	Accuracy	Range	False max	Width	Noise level	Overall score
F-1 ThresholdAbsGrad	2.67 (9)	417.00 (7)	131.00 (12)	16.17 (5)	0.0225 (5)	1.1979 (7)
F-2 SquaredGradient	2.50 (5)	428.50 (9)	129.50 (11)	15.33 (4)	0.0325 (8)	1.2083 (8)
F-3 BrennerGradient	2.42 (3)	408.92 (5)	121.17 (9)	14.08 (3)	0.0246 (6)	1.1425 (5)
F-4 TenenbaumGradient	2.42 (3)	406.00 (4)	119.33 (8)	14.00 (2)	0.0224 (4)	1.1303 (4)
F-5 ModifiedLaplace	38.42 (14)	462.08 (13)	148.00 (16)	37.67 (8)	0.2763 (15)	1.4048 (13)
F-6 EnergyLaplace	2.00 (1)	459.67 (12)	141.25 (13)	32.58 (6)	0.1438 (11)	1.3158 (9)
F-7 Wavelet_1	38.50 (15)	465.67 (14)	152.58 (17)	37.58 (7)	0.3649 (16)	1.4301 (14)
F-8 Wavelet_2	26.75 (12)	469.50 (16)	142.83 (14)	54.75 (10)	0.2533 (14)	1.3851 (12)
F-9 Wavelet_3	26.75 (12)	467.08 (15)	143.25 (15)	50.25 (9)	0.1798 (13)	1.3776 (10)
F-10 Variance	2.58 (6)	135.92 (3)	16.00 (3)	67.50 (13)	0.0029 (3)	0.4813 (3)
F-11 NormedVariance	2.58 (6)	125.50 (1)	12.83 (1)	66.92 (12)	0.0027 (2)	0.4626 (1)
F-12 AutoCorrelation	2.25 (2)	416.33 (6)	126.83 (10)	13.42 (1)	0.0278 (7)	1.1777 (6)
F-13 StdDevCorr	2.58 (6)	126.83 (2)	13.08 (2)	69.08 (14)	0.0026 (1)	0.4742 (2)
F-14 Range	10.33 (11)	477.50 (17)	118.25 (7)	101.42 (15)	1.0535 (17)	1.3787 (11)
F-15 Entropy	7.42 (10)	484.92 (18)	158.08 (18)	63.75 (11)	5.2433 (18)	1.7698 (18)
F-16 AboveThreshold	86.25 (17)	456.33 (10)	77.42 (5)	128.83 (17)	0.1205 (10)	1.5359 (16)
F-17 PixelCount	102.00 (18)	422.25 (8)	54.83 (4)	179.00 (18)	0.1585 (12)	1.6969 (17)
F-18 ImagePower	84.50 (16)	458.67 (11)	80.42 (6)	121.75 (16)	0.1183 (9)	1.5175 (15)

Each entry is based on 18 image sets under ***bright field*** and averaged. No image preprocessing was conducted.

TABLE 6. Ranking of the 18 focus algorithms according to individual criterion distance and overall score

Algorithm	Accuracy	Range	False max	Width	Noise level	Overall score
F-1 ThresholdAbsGrad	2.58 (9)	381.83 (4)	73.17 (10)	23.17 (8)	0.0244 (4)	0.9251 (6)
F-2 SquaredGradient	3.33 (11)	421.58 (10)	85.58 (11)	16.00 (2)	0.0382 (9)	1.0338 (8)
F-3 BrennerGradient	2.50 (6)	395.08 (5)	64.67 (7)	16.17 (3)	0.0354 (7)	0.9200 (5)
F-4 TenenbaumGradient	2.50 (6)	399.67 (6)	60.83 (5)	16.33 (4)	0.0335 (6)	0.9177 (4)
F-5 ModifiedLaplace	4.17 (13)	443.67 (12)	124.83 (16)	16.67 (5)	0.0624 (11)	1.2213 (14)
F-6 EnergyLaplace	2.50 (6)	437.92 (11)	114.08 (13)	16.67 (5)	0.0733 (13)	1.1675 (10)
F-7 Wavelet_1	4.83 (15)	448.67 (15)	128.33 (17)	17.42 (7)	0.0850 (14)	1.2444 (15)
F-8 Wavelet_2	2.08 (3)	445.08 (13)	117.50 (15)	37.42 (10)	0.2070 (16)	1.2034 (13)
F-9 Wavelet_3	2.33 (5)	446.33 (14)	115.83 (14)	31.50 (9)	0.1117 (15)	1.1943 (12)
F-10 Variance	1.92 (1)	166.75 (3)	7.92 (3)	45.75 (12)	0.0063 (3)	0.4040 (3)
F-11 NormedVariance	1.92 (1)	142.75 (1)	6.42 (1)	44.75 (11)	0.0063 (2)	0.3588 (1)
F-12 AutoCorrelation	2.58 (9)	403.67 (7)	69.92 (9)	15.67 (1)	0.0359 (8)	0.9510 (7)
F-13 StdDevCorr	2.08 (3)	160.42 (2)	7.58 (2)	47.25 (13)	0.0054 (1)	0.3962 (2)
F-14 Range	4.42 (14)	474.00 (16)	105.33 (12)	160.00 (17)	0.4749 (17)	1.3950 (16)
F-15 Entropy	3.92 (12)	483.25 (18)	155.92 (18)	102.00 (14)	3.2472 (18)	1.7907 (18)
F-16 AboveThreshold	41.67 (17)	416.00 (9)	61.83 (6)	131.50 (16)	0.0418 (10)	1.1890 (11)
F-17 PixelCount	99.67 (18)	474.67 (17)	65.25 (8)	225.33 (18)	0.0656 (12)	1.7721 (17)
F-18 ImagePower	40.67 (16)	415.75 (8)	57.17 (4)	106.08 (15)	0.0290 (5)	1.1237 (9)

Each entry is based on 18 image sets under ***phase contrast*** and averaged. No image preprocessing was conducted.

TABLE 7. Ranking of the 18 focus algorithms according to individual criterion distance and overall score

Algorithm	Accuracy	Range	False max	Width	Noise level	Overall score
F-1 ThresholdAbsGrad	3.25 (4)	414.08 (10)	127.50 (13)	15.75 (4)	0.0218 (7)	1.1955 (10)
F-2 SquaredGradient	3.25 (4)	423.42 (11)	115.92 (10)	18.92 (5)	0.0372 (11)	1.1607 (8)
F-3 BrennerGradient	3.17 (1)	398.25 (8)	108.67 (9)	15.50 (3)	0.0316 (10)	1.0896 (7)
F-4 TenenbaumGradient	3.17 (1)	391.42 (7)	106.67 (8)	14.83 (2)	0.0292 (8)	1.0702 (6)
F-5 ModifiedLaplace	4.42 (10)	458.00 (15)	145.67 (17)	36.00 (6)	0.0848 (15)	1.3509 (13)
F-6 EnergyLaplace	39.42 (13)	453.00 (12)	127.92 (15)	42.33 (8)	0.0593 (12)	1.3592 (14)
F-7 Wavelet_1	4.75 (12)	457.17 (14)	145.25 (16)	36.00 (6)	0.0885 (16)	1.3480 (12)
F-8 Wavelet_2	59.58 (17)	460.83 (16)	126.75 (12)	57.58 (17)	0.0663 (14)	1.4842 (16)
F-9 Wavelet_3	39.42 (13)	456.08 (13)	127.67 (14)	43.17 (10)	0.0630 (13)	1.3632 (15)
F-10 Variance	3.83 (7)	158.25 (2)	19.08 (5)	42.50 (9)	0.0061 (3)	0.3998 (3)
F-11 NormedVariance	3.67 (6)	148.50 (1)	19.42 (6)	43.75 (12)	0.0061 (2)	0.3863 (1)
F-12 AutoCorrelation	3.17 (1)	410.58 (9)	122.67 (11)	13.17 (1)	0.0302 (9)	1.1682 (9)
F-13 StdDevCorr	3.83 (7)	159.00 (3)	17.08 (3)	43.50 (11)	0.0053 (1)	0.3993 (2)
F-14 Range	4.58 (11)	465.00 (17)	105.58 (7)	55.75 (15)	0.2623 (17)	1.2143 (11)
F-15 Entropy	4.33 (9)	480.75 (18)	154.50 (18)	51.00 (13)	2.5786 (18)	1.7469 (18)
F-16 AboveThreshold	40.75 (16)	338.92 (6)	16.08 (1)	55.33 (14)	0.0126 (4)	0.9064 (5)
F-17 PixelCount	80.50 (18)	328.00 (5)	17.25 (4)	230.67 (18)	0.0144 (6)	1.5742 (17)
F-18 ImagePower	40.50 (15)	326.75 (4)	16.17 (2)	56.08 (16)	0.0129 (5)	0.8861 (4)

Each entry is based on 18 image sets under ***DIC*** and averaged. No image preprocessing was conducted.

1) 100% (no subsampling)
2) 80% subsampling of each image dimension
3) 50% subsampling of each image dimension
4) 20% subsampling of each image dimension
5) 5% subsampling of each image dimension
6) 9 by 9 binomial filter on entire images
7) noise filter with an intensity amplitude of 40 for adding random noise

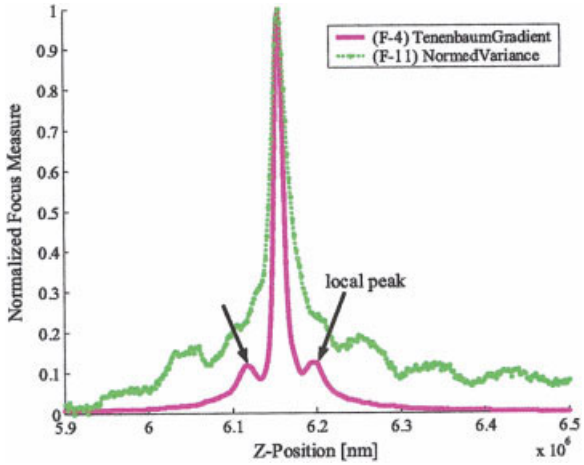

Fig. 5. Tenenbaum Gradient (F-4) and Normalized Variance (F-11) on 5% subsampled images under phase contrast. Phase transition effect is clearly visible with the two local peaks around the global peak. [Color figure can be viewed in the online issue, which is available at www.interscience.wiley.com.]

TABLE 9. Execution time decreases as more subsampling is applied

Algorithm	100% sampled	80% sampled	50% sampled
F-1 ThresholdAbsGrad	17 ms	10 ms	4 ms
F-2 SquaredGradient	16 ms	10 ms	4 ms
F-3 BrennerGradient	19 ms	11 ms	3 ms
F-4 TenenbaumGradient	30 ms	19 ms	7 ms
F-5 ModifiedLaplace	18 ms	12 ms	4 ms
F-6 EnergyLaplace	33 ms	21 ms	8 ms
F-7 Wavelet_1	10 ms	8 ms	5 ms
F-8 Wavelet_2	16 ms	12 ms	6 ms
F-9 Wavelet_3	16 ms	12 ms	6 ms
F-10 Variance	7 ms	4 ms	2 ms
F-11 NormedVariance	7 ms	4 ms	1 ms
F-12 AutoCorrelation	4 ms	3 ms	1 ms
F-13 StdDevCorr	5 ms	3 ms	1 ms
F-14 Range	3 ms	2 ms	<1 ms
F-15 Entropy	6 ms	4 ms	1 ms
F-16 AboveThreshold	4 ms	2 ms	1 ms
F-17 PixelCount	3 ms	2 ms	1 ms
F-18 ImagePower	5 ms	3 ms	1 ms

TABLE 8. Ranking of the 18 focus algorithms according to individual criterion distance and overall score

Algorithm	Accuracy	Range	False max	Width	Noise level	Overall score
F-1 ThresholdAbsGrad	2.81 (2)	464.69 (7)	146.50 (11)	18.92 (6)	0.4915 (6)	1.3417 (3)
F-2 SquaredGradient	24.03 (11)	469.81 (9)	147.61 (12)	42.78 (9)	1.1759 (9)	1.3880 (5)
F-3 BrennerGradient	2.86 (3)	463.33 (6)	145.14 (10)	18.69 (5)	0.3269 (3)	1.3336 (2)
F-4 TenenbaumGradient	2.69 (1)	448.06 (4)	126.22 (6)	19.83 (7)	0.0443 (1)	1.2306 (1)
F-5 ModifiedLaplace	3.31 (4)	473.64 (12)	154.25 (14)	22.11 (8)	3.3948 (14)	1.3966 (7)
F-6 EnergyLaplace	60.89 (15)	476.81 (15)	149.97 (13)	69.22 (10)	1.4658 (13)	1.5364 (16)
F-7 Wavelet_1	11.72 (9)	476.67 (14)	156.28 (16)	10.31 (3)	11.0570 (17)	1.4711 (12)
F-8 Wavelet_2	4.14 (5)	476.86 (16)	156.61 (17)	8.14 (1)	9.5613 (16)	1.4520 (11)
F-9 Wavelet_3	14.22 (10)	475.72 (13)	155.33 (15)	8.19 (2)	8.9282 (15)	1.4448 (10)
F-10 Variance	54.11 (13)	471.67 (10)	128.53 (8)	132.72 (15)	0.4494 (5)	1.5273 (13)
F-11 NormedVariance	38.97 (12)	461.50 (5)	121.44 (4)	109.00 (14)	0.1929 (2)	1.3947 (6)
F-12 AutoCorrelation	10.58 (8)	480.56 (18)	158.42 (18)	12.00 (4)	25.2867 (18)	1.7362 (17)
F-13 StdDevCorr	54.33 (14)	468.83 (8)	125.31 (5)	140.06 (16)	0.3617 (4)	1.5295 (14)
F-14 Range	6.36 (7)	477.22 (17)	126.36 (7)	91.67 (12)	1.2288 (10)	1.3535 (4)
F-15 Entropy	5.56 (6)	473.25 (11)	142.25 (9)	153.92 (17)	1.2852 (12)	1.5346 (15)
F-16 AboveThreshold	73.72 (17)	440.56 (3)	106.58 (3)	96.19 (13)	0.8663 (8)	1.4306 (9)
F-17 PixelCount	101.42 (18)	436.17 (2)	90.64 (1)	203.31 (18)	1.2815 (11)	1.7759 (18)
F-18 ImagePower	73.42 (16)	434.58 (1)	105.50 (2)	87.36 (11)	0.6105 (7)	1.4038 (8)

Each entry is based on 36 image sets and averaged. ***5% subsampling*** was conducted.

It should be noted that in experiments the magnitudes of the binomial and noise filter were set to fairly large values in order to more visibly reveal the preprocessing effects.

Table 8 summarizes the effect of subsampling on the criterion distances and overall scores. By comparing Tables 2 (100% subsampled) and 8 (5% subsampled), one can see that (Normalized) Variance (F-10 and F-11) and Correlation-based algorithms (F-12 and F-13) are very sensitive to subsampling. These algorithms (F-10–F-12) appear to behave as the Wavelet-based algorithms for 100% subsampled images shown in Figure 4, producing poor accuracy distances. The AutoCorrelation algorithm (F-12) does not exhibit this behavior, but it responds to subsampling with a very high noise level. Generally, noise level was found to become worse for subsampled images because less information appears in the subsampled images. Widths remain relatively constant for the Wavelet-based algorithms (F-7–F-9). These algorithms (F-7–F-9) rank the best in terms of widths, making them well suited for image segmentation purposes (Yang and Nelson, 2003a). From Table 9, one can also find that subsampling dramatically reduces execution time.

Tenenbaum Gradient (F-4) was found to provide the best overall performance on subsampled (below 80%) images because (F-4) uses more neighboring pixels than other algorithms such as Normalized Variance (F-11), which makes it more robust to the reduced information content from subsampling. As shown in Figure 5, (F-4) still performs satisfactorily on 5% subsampled images compared to (F-11). The two local peaks around the global peak are due to the phase transition effect.

Table 10 summarizes the effect of random noise on the criterion distances and overall score. By comparing Table 2 (no random noise added) and Table 10, one can see that the noise level increases dramatically when random noise is added. The criterion distances of false maxima and width also deteriorate. The accuracy of

TABLE 10. Ranking of the 18 focus algorithms according to individual criterion distance and overall score

Algorithm	Accuracy	Range	False max	Width	Noise level	Overall score
F-1 ThresholdAbsGrad	14.36 (9)	465.44 (9)	149.50 (11)	23.36 (5)	0.7931 (10)	1.3486 (8)
F-2 SquaredGradient	14.31 (8)	466.78 (10)	149.78 (12)	19.92 (4)	1.1799 (11)	1.3512 (9)
F-3 BrennerGradient	2.28 (1)	455.36 (6)	142.03 (9)	14.42 (2)	0.1985 (6)	1.2956 (6)
F-4 TenenbaumGradient	2.67 (2)	450.50 (5)	141.08 (8)	14.86 (3)	0.1263 (4)	1.2843 (5)
F-5 ModifiedLaplace	50.19 (14)	478.44 (14)	156.00 (13)	55.69 (13)	8.6193 (15)	1.4875 (14)
F-6 EnergyLaplace	35.03 (10)	477.06 (13)	156.08 (14)	44.42 (8)	7.8085 (14)	1.4534 (12)
F-7 Wavelet_1	44.11 (12)	479.97 (16)	159.44 (15)	31.72 (6)	24.4682 (18)	1.7537 (17)
F-8 Wavelet_2	67.33 (16)	479.97 (16)	159.94 (17)	39.78 (7)	17.0374 (17)	1.6379 (16)
F-9 Wavelet_3	63.50 (15)	479.31 (15)	159.44 (15)	49.86 (9)	9.2687 (16)	1.5259 (15)
F-10 Variance	2.75 (3)	410.22 (1)	99.69 (2)	52.69 (10)	0.0191 (3)	1.0763 (2)
F-11 NormedVariance	2.75 (3)	410.33 (2)	99.17 (1)	53.03 (11)	0.0186 (2)	1.0749 (1)
F-12 AutoCorrelation	2.78 (6)	460.44 (7)	145.64 (10)	14.22 (1)	0.5987 (9)	1.3189 (7)
F-13 StdDevCorr	2.75 (3)	411.17 (3)	99.92 (3)	54.17 (12)	0.0185 (1)	1.0800 (3)
F-14 Range	35.94 (11)	476.25 (12)	113.67 (7)	173.72 (17)	2.4873 (12)	1.4446 (11)
F-15 Entropy	11.06 (7)	483.72 (18)	159.97 (18)	72.64 (14)	7.6654 (13)	1.4830 (13)
F-16 AboveThreshold	86.17 (17)	460.44 (7)	106.53 (5)	128.25 (16)	0.2410 (8)	1.3971 (10)
F-17 PixelCount	156.64 (18)	474.39 (11)	110.69 (6)	234.31 (18)	0.2227 (7)	1.8549 (18)
F-18 ImagePower	47.69 (13)	442.53 (4)	101.50 (4)	108.17 (15)	0.1484 (5)	1.2431 (4)

Each entry is based on 36 image sets and averaged. ***Random noise*** was added.

TABLE 11. Ranking of the 18 focus algorithms according to individual criterion distance and overall score

Algorithm	Accuracy	Range	False max	Width	Noise level	Overall score
F-1 ThresholdAbsGrad	2.89 (7)	340.22 (4)	70.17 (9)	26.50 (10)	0.0080 (4)	0.8423 (4)
F-2 SquaredGradient	2.83 (5)	368.61 (7)	75.08 (11)	16.78 (4)	0.0153 (8)	0.9027 (7)
F-3 BrennerGradient	2.83 (5)	364.69 (6)	72.92 (10)	17.11 (7)	0.0146 (6)	0.8888 (6)
F-4 TenenbaumGradient	2.78 (3)	361.06 (5)	69.69 (7)	17.08 (6)	0.0142 (5)	0.8719 (5)
F-5 ModifiedLaplace	2.78 (3)	435.00 (13)	109.94 (14)	24.00 (8)	0.0299 (9)	1.1440 (12)
F-6 EnergyLaplace	2.47 (1)	426.56 (12)	108.75 (13)	16.61 (3)	0.0343 (10)	1.1226 (9)
F-7 Wavelet_1	3.00 (9)	449.19 (14)	122.69 (15)	24.44 (9)	0.0517 (12)	1.2174 (14)
F-8 Wavelet_2	3.33 (12)	456.58 (17)	136.31 (17)	16.36 (2)	0.1080 (17)	1.2829 (16)
F-9 Wavelet_3	2.94 (8)	453.33 (16)	130.08 (16)	17.03 (5)	0.0619 (14)	1.2515 (15)
F-10 Variance	3.28 (11)	159.14 (2)	12.78 (2)	61.14 (12)	0.0023 (3)	0.4464 (2)
F-11 NormedVariance	3.14 (10)	139.92 (1)	11.14 (1)	60.94 (11)	0.0021 (1)	0.4153 (1)
F-12 AutoCorrelation	2.72 (2)	373.47 (8)	80.25 (12)	16.33 (1)	0.0153 (7)	0.9285 (8)
F-13 StdDevCorr	3.42 (13)	159.14 (2)	12.81 (3)	61.92 (13)	0.0022 (2)	0.4489 (3)
F-14 Range	6.53 (15)	451.97 (15)	70.14 (8)	97.47 (15)	0.1080 (16)	1.1350 (11)
F-15 Entropy	5.47 (14)	483.39 (18)	157.83 (18)	70.61 (14)	3.9902 (18)	1.7646 (18)
F-16 AboveThreshold	52.19 (16)	385.06 (10)	51.19 (5)	118.33 (17)	0.0515 (11)	1.1488 (13)
F-17 PixelCount	100.81 (18)	407.67 (11)	51.94 (6)	211.92 (18)	0.0833 (15)	1.6793 (17)
F-18 ImagePower	55.25 (17)	378.58 (9)	50.31 (4)	105.08 (16)	0.0541 (13)	1.1231 (10)

Each entry is based on 36 image sets and averaged. ***Low pass filtering*** was applied.

algorithms (F-4, F-10, F-11) and (F-13) is fairly constant, demonstrating their robustness to noise.

Table 11 summarizes the effect of low-pass filtering as a preprocessing operation on the criterion distances and overall score. By comparing Table 2 (no low-pass preprocessing) and Table 11, one can see that the noise level decreases dramatically when low-pass preprocessing is applied to images. Accuracy and widths are improved for algorithms (F-5–F-9).

CONCLUSION

This article presents a comprehensive comparison study of 18 focus algorithms by processing a total of 139,000 microscope images. Six samples were used with three observation methods (brightfield, phase contrast, and differential interference contrast (DIC)) under two magnifications (100× and 400×). A ranking methodology was proposed, based on which the 18 focus algorithms were ranked. Image preprocessing was also conducted to extensively reveal the performance and robustness of the focus algorithms. Based on the observations presented in the Results and Discussion section, one may conclude the following guidelines for selecting the optimal focus algorithm.

1) For all three observation methods (i.e., brightfield, phase contrast, and DIC), Normalized Variance (F-11) provides the best overall performance. Although AutoCorrelation (F-12) was found to be the optimal algorithm for fluorescence microscopy applications (3), it was not found to be capable of providing the best performance under brightfield, phase contrast, or DIC.
2) When images are subsampled in order to increase execution speed, gradient-based focus algorithms should be selected, among which Tenenbaum Gradient (F-4) was found to provide the best overall performance.
3) When images are noisy, Normalized Variance (F-11) is the most satisfactory due to its robustness to noise.
4) If low-pass filtering is applied as a preprocessing operation, Normalized Variance (F-11) is also capable of providing the best overall performance.

These general guidelines together with the observations presented in the Results and Discussion section allow for selecting the optimal focus algorithm for different microscopy applications. If more attention must be paid to a specific criterion instead of the overall

performance under a particular set of conditions, for example, width for 5% subsampled images for image segmentation purposes, one can find that the Wavelet-based focus algorithm (F-8) should be chosen by referring to Table 8.

REFERENCES

Brenner JF, Dew BS, Horton JB, King JB, Neirath PW, Sellers WD. 1971. An automated microscope for cytologic research. J Histochem Cytochem 24:100–111.

Firestone L, Cook K, Culp K, Talsania N, Preston K. 1991. Comparison of autofocus methods for automated microscopy. Cytometry 12:195–206.

Groen F, Young IT, Ligthart G. 1985. A comparison of different focus functions for use in autofocus algorithms. Cytometry 12: 81–91.

Krotov E. 1987. Focusing. Int J Comput Vis 1:223–237.

Mendelsohn ML, Mayall BH. 1972. Computer-oriented analysis of human chromosomes — III focus. Comput Biol Med 2:137–150.

Nayar SK, Nakagawa Y. 1994. Shape from Focus. IEEE Trans Pattern Anal Machine Intell 16:824–831.

Santos A, Solórzano CO, Vaquero JJ, Peña JM, Malpica N, Pozo F. 1997. Evaluation of autofocus functions in molecular cytogenetic analysis. J Microsc 188:264–272.

Subbarao M, Choi TS, Nikzad A. 1993. Focusing techniques. J Opt Eng 32:824–2836.

Yang G, Nelson BJ. 2003a. Wavelet-based auto-focusing and unsupervised segmentation of microscopic images. Proc IEEE/RSJ International Conference on Intelligent Robots and Systems 2143–2148.

Yang G, Nelson BJ. 2003b. Micromanipulation contact transition control by selective focusing and microforce control. Proc IEEE International Conference on Robotics and Automation 3200–3206.

Vollath D. 1987. Automatic focusing by correlative methods. J Microsc 147:279–288.

Vollath D. 1988. The influence of the scene parameters and of noise on the behavior of automatic focusing algorithms. J Microsc 151:133–146.

Yeo T, Jayasooriah SO, Sinniah R. 1993. Autofocusing for tissue microscopy. Image Vis Comput 11:629–639.